Experimental Validation of a Mesh-to-Mesh Magnetic Force Projection for e-NVH Simulation

Raphaël Pile, Jean Le Besnerais, Guillaume Parent, Martin Glesser, Yvonnick Le Menach

Experimental Validation of a Mesh-to-Mesh Magnetic Force Projection for e-NVH Simulation

Raphaël Pile[1], Jean Le Besnerais[2], Guillaume Parent[1], Martin Glesser[2], and Yvonnick Le Menach[3]
[1]Univ. Artois, UR 4025, Laboratoire Systèmes Electrotechniques et Environnement (LSEE), F-62400 Béthune, France
[2]EOMYS ENGINEERING, Villeneuve d'Ascq, France
[3]Univ. Lille, Arts et Métiers Institute of Technology, Centrale Lille, Junia, ULR2697-L2EP, Lille, France

This article discusses the use of simulation for analyzing the vibro-acoustic behavior of radial flux electrical machines under magnetic forces. Numerical simulation enables a systematic investigation of electromagnetic Noise, Vibration and Harshness (e-NVH) issues, but requires accurate modeling and this despite manufacturing uncertainties. Experimental validation is a necessary step to setup a multiphysic virtual prototyping e-NVH workflow. In particular, a key point is the magneto-mechanical coupling. In this study, the Virtual Work Principle (VWP) is used for magnetic force calculation. The goal is to propose an accurate e-NVH model applied to a 12s10p radial flux electrical machine using a mesh-to-mesh projection. This e-NVH model enables to understand the origin of the noisiest orders along the whole speed range of the machine. Differences between simulation and experiments are discussed thanks to the modal participation factor of specific harmonics. Mesh-to-mesh projection results are compared to those obtained by using lumped tooth force, highlighting the contribution of the tooth tip moment to the vibration. Finally, the tooth modulation effect is discussed in the light of these results.

***Index Terms*—electrical machines, virtual work principle, magnetic forces, mesh-to-mesh projection, vibrations.**

I. Introduction

THE analysis of the vibro-acoustic behavior of electrical machines is the subject of many research such as about virtual prototyping [1], experimental e-NVH benchmark [2], or mechanical modelling [3]. The problem is even increased insofar as the mass and volume power optimization impacts the vibration and noise levels. These phenomena must be taken into account from the design stage by means of multiphysics simulations. Simulation enables a more controlled and systematic investigation of noise and vibration issues. It can be used to study the effect of various parameters (e.g. slot/pole combination, teeth/magnets shape, magnetic and mechanical material properties...) on the acoustic performance of the machine. The Finite Element (FE) method is particularly suitable for the detailed study of different topologies, whether for electromagnetism or structural mechanics aspects. The presented study is therefore positioned in this context, with the use of FE for both physics. Then, a key point of the e-NVH numerical model is the magneto-mechanical coupling.

In many related scientific works [3], [4], the Maxwell stress tensor method is used to estimate the magnetic force distribution based on the airgap magnetic field. In most of the numerical simulation, this magnetic force distribution is integrated over one slot pitch to obtain lumped tooth forces. These radial, tangential lumped forces (and sometimes lumped moment) are then applied onto the mechanical FE model at the middle point of the tip of the teeth. By construction, the method based on lumped force cannot account for force distribution on the teeth and the consequence on the vibration.

To take into account the distribution of magnetic force on the lamination, another method consists in the projection of the force distribution onto the mechanical mesh (used for modal analysis) using a Galerkin mesh-to-mesh method [1], [5]. Indeed, the electromagnetic mesh of the stator is significantly finer than the mechanical mesh, which is too computationally costly for e-NVH analysis and optimization.

The Virtual Work Principle (VWP) is a more accurate method to compute magnetic forces [6]. This study proposes to perform a complete e-NVH simulation using VWP and mesh-to-mesh projection as in [5]. The novelty of this study is to use the VWP based prediction in order to discuss the accuracy of the lumped force method independantly for different orders. This study is performed on a 12s10p radial flux Surface Permanent Magnet Synchronous Machine (SPMSM) specifically designed to study e-NVH issues [2]. This machine have low saturation levels, such that only magnetic surface forces are considered in the study.

Simulation may not take into account real-world factors such as operating temperature, manufacturing tolerances and wear and tear on the machine, which can affect its performance. It is particularly the case for noise and vibration issues. Thus, an experimental validation is a necessary step to fully understand e-NVH phenomena, and in particular to validate the magneto-mechanical coupling. This study proposes to validate the proposed e-NVH model by comparing experimental and numerical vibration levels at specific orders:

- at twice times the electrical frequency, $2f_s$, because it is dominating the e-NVH response in forced condition,
- at ten times the electrical frequency, $10f_s$, because it is responsible for an acoustic resonance.

Then, the results are compared with the case where lumped forces (one resultant per tooth) are used instead. The novelty of the study is also that it examines the impact of moment resultant on the vibration. Lastly, the vibration results are decomposed by modal projection factor. Comparison between $2f_s$ and $10f_s$ supports the existence of the tooth modulation effect in a 12s10p machine as presented in [4].

II. Magnetic Force Projection

A. Virtual Work Principle

Let Γ be the domain of definition of the electromagnetic problem, and $\mathbb{M}$ the meshing of this domain. In the Virtual Work Method (VWP) corresponding, the resultant magnetic force F_s^i (related to the spatial direction $s \in \{\mathbf{x}, \mathbf{y}, \mathbf{z}\}$) on the i$^{\text{th}}$ node of $\mathbb{M}$ is calculated with a balance of magnetic co-energy on the cells e surrounding the node [6], [7]. In the magnetically linear case, the nodal force can be expressed as:

$$F_s^i = \sum_{\forall e | i \in e} \int_e \left(-\mathbf{B}^T \cdot \mathbb{J}^{-1} \cdot \frac{\partial \mathbb{J}}{\partial s} \cdot \mathbf{H} + \frac{\mu}{2} |\mathbf{H}|^2 \ |\mathbb{J}^{-1}| \ \frac{\partial |\mathbb{J}|}{\partial s} \right) \mathrm{d}e \tag{1}$$

where $\mathbf{H}$ is the magnetic field, $\mathbf{B}$ the magnetic flux density, $\mathbb{J}$ the Jacobian matrix of each element, $|\mathbb{J}|$ its determinant, and $|\mathbb{J}^{-1}|$ its inverse determinant. F_s^i is expressed in Newton (or Newton per unit length in 2D) and is proportional to the size of the surrounding elements: bigger elements implies more integrated magnetic co-energy. Moreover, the calculation of the Jacobian derivative $\frac{\partial |\mathbb{J}|}{\partial s}$ depends on the (virtually) moving node (i). In the following, the matrix of the coordinates of the element nodes is denoted S, and the matrix of shape functions in the element of reference is ω_{ref} (i.e. usually a normalized element where the shape functions are analytically defined). The Jacobian matrix between an element and the reference element can be expressed as [6]:

$$\mathbb{J} = \nabla \omega_{\text{ref}} S \tag{2}$$

The derivatives of (2) can then be computed depending on the considered node (i):

$$\frac{\partial \mathbb{J}}{\partial s}^{(i)} = \frac{\partial \nabla \omega_{\text{ref}}}{\partial s} S + \nabla \omega_{\text{ref}} \frac{\partial S}{\partial s}^{(i)} \tag{3}$$

The first term of (3) can be derived analytically from the expression of the shape functions in the reference element. However, the second term is not straightforward. The idea proposed by [6] is to virtually perform an elementary displacement of each node. Thus, the derivative now depends on the targeted node (i) and denoted $\frac{\partial}{\partial s}^{(i)}$. The matrix $\frac{\partial S}{\partial s}^{(i)}$ is equal to zero everywhere except for one value - at the i^{th} line and column corresponding to the spatial direction s - equal to one. The calculation of the determinant derivative relies on the same principle. In order to compute the determinant derivative, it is proposed to use the trace operator:

$$\frac{\partial |\mathbb{J}|}{\partial s}^{(i)} = \mathrm{Tr}\left(\mathbb{J}^{-1} \frac{\partial \mathbb{J}}{\partial s}^{(i)} \right) |\mathbb{J}| \tag{4}$$

This last equation was not found in the analysed literature, but it simplifies calculations and implementation since the derivatives of the jacobian determinant can be expressed as a function of (3) and (2).

The direction notation s is omitted in the following sections since all equations can be put under a vectorial form.

B. Mesh-to-Mesh Projection

This section gives the main steps of the mesh-to-mesh projection method used in this study. More details on the different parameters and their effects are given in [5], [8]. First, all the nodal resultants on the magnetic mesh F^i are computed according to (1). Assuming that the nodal resultants come from a continuous force field f defined on a discrete shape function basis ψ_i associated to the magnetic surface mesh (at the interface between air and lamination or between windings and lamination) such that

$$f = \sum_{k=1}^{N} \psi_k f_k \tag{5}$$

then the link between F^i and f is the integration of the force field interpolated by all the shape functions [9]:

$$\sum_{k=1}^{\mathrm{N}} f_k \int \psi_i \psi_k \ d\tau = F^i \tag{6}$$

where N is the total number of nodes. Considering all the possible combinations of i and k, (6) leads to a linear matrix system of size N to be solved:

$$[A][f] = [F] \tag{7}$$

with

$$A_{i,k} = \int \psi_i \psi_k \ d\tau \tag{8}$$

The next step is using a Ritz-Galerkin mesh-to-mesh projection method [1], [5], [9] on the calculated magnetic surface force density f in order to obtain the equivalent force density $\hat{f}$ on the mechanical mesh. This comes down to solving the following linear matrix problem:

$$[C][\hat{f}] = [f^*] \tag{9}$$

with

$$C_{j,k} = \int \phi_j \phi_k \ d\tau \tag{10}$$

where ϕ represents the shape functions of the mechanical mesh, and the components f_j^* of $[f^*]$ computed according to

$$f_j^* = \sum_{i=1}^{N} f_i \int \phi_j \psi_i \ d\tau \tag{11}$$

The last step of the mesh-to-mesh projection is to compute the nodal force components $\hat{F}^j$ of the matrix $\hat{F}$ on the mechanical mesh with

$$\hat{F}^j = \sum_{k=1}^{\mathrm{N}} \hat{f}_k \int \phi_j \phi_k \ d\tau \tag{12}$$

The matrix of the nodal forces on all nodes and in every directions is noted $\hat{\mathbf{F}}$ in the following sections. The question of the preservation of the value of the lumped forces is discussed in [8]. The algorithm can be generalized to volumic force density, as long as the shape function ψ_i and ϕ_j are both defined in 3D.

C. Modal Superpostion

The goal of this section is to present the method used to compute the vibration based on the electromagnetic forces. An eigenfrequency analysis is performed on the mechanical FE model to obtain M eigenmodes with corresponding modal displacement $\mathbf{Q}_i$. The corresponding Frequency Response Function (FRF) can be synthesized according to the modal superposition method [10], [11]:

$$\mathbf{X}(\omega) = \sum_{n=1}^{\mathrm{M}} \mathbf{Q}_n \frac{\mathbf{Q}_n \cdot \hat{\mathbf{F}}(\omega)}{\omega_n + 2j\omega\epsilon_n\omega_n - \omega^2} \tag{13}$$

where the scalar $\mathbf{Q}_n \cdot \hat{\mathbf{F}}(\omega)$ is the modal projection factor as it represents the capacity of the magnetic excitation to interact with each mode shape. The damping ϵ_n is assumed equal to 0.2% for all modes. The result $\mathbf{X}(\omega)$ corresponds to the vibration obtained by applying the magnetic force (12) on selected nodes of the modal basis. The method is valid under the assumption of mechanical linearity which is commonly used for e-NVH studies considering the small displacements implied.

III. Application to 12S10P SPMSM

The simulations and analyses are performed on the 12s10p SPMSM machine described in [2] in which only magnetic surface force are considered due to very low magnetic saturation. The magnetic field is solved using 2D non-linear magneto-static FE analysis with MANATEE-FEMM coupling [12]. First, the physical origin of each magnetic excitation is analysed in Section III-A. This first analysis is used to understand numerical and experimental results obtained in Section III-B. Finally, the mesh-to-mesh results are used to discuss magneto-mechanical coupling based on lumped force and tooth modulation effect.

A. Analysis of the Maxwell Stress Spectrum

In this section, the magnetic force spectrum predicted by the Maxwell stress tensor method is presented. It is used in the next section to analyze and understand the difference between experimental and numerical results.

The Maxwell stress method is initially an accurate method to compute the global unbalanced forces and torque applying on the machine. It has been extended to the estimation of the local forces. The radial and circumferential force distributions are computed in the airgap according to

$$\mathrm{P_r}(\theta,t) = -\frac{1}{2\mu_0}\left(\mathrm{B_r^2}(\theta,t) - \mathrm{B_\theta^2}(\theta,t)\right) \tag{14}$$

$$\mathrm{P_\theta}(\theta,t) = -\frac{1}{2\mu_0}\mathrm{B_r}(\theta,t)\,\mathrm{B_\theta}(\theta,t) \tag{15}$$

where θ is the angular position in the airgap, $\mathrm{B_r}$ the radial magnetic flux density, and $\mathrm{B_\theta}$ the circumferential magnetic flux density. This method gives interpretable results which are accurate enough for eNVH pre-design phase when computing lumped tooth force [3]. The 2D Fourier transform of (14) is illustrated in Fig. 1. The main magnetic force harmonic is at twice the electrical frequency $2\mathrm{f_s}$ and a resonance of $10\mathrm{f_s}$ with the ovalization modes (2,0) is also expected within the speed range [2]. Hence, these harmonics are used to test the proposed approach of mesh-to-mesh projection in the next sections. Both 10fs and 2fs are composed of a combination of wavenumbers $r = \pm 10$ and $r = \pm 2$.

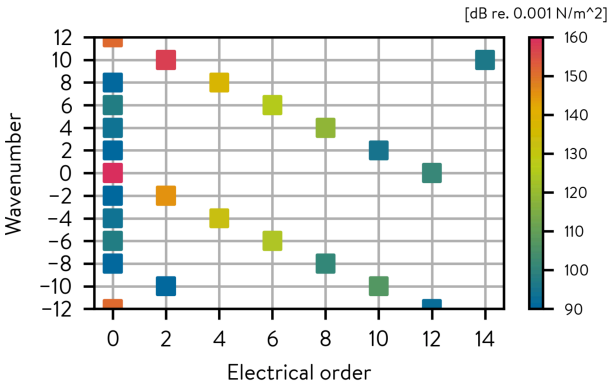

Fig. 1: Fourier transform (time and angle) of the airgap surface force from the Maxwell stress tensor method.

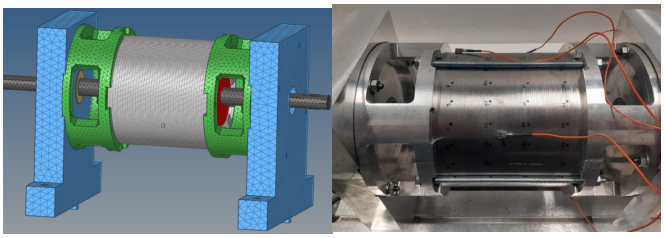

(a) FE model (b) Experimental set-up

Fig. 2: Benchmark test bed

TABLE I: Numerical and experimental modal analysis of the mounted benchmark with the 12s10p machine. Only significant stator modes are reported.

Mode Number	Mode identification	Natural Frequency (numerical) [Hz]	Natural Frequency (experimental) [Hz]
1	(2,0)	708	721
2	(2,0)	727	797
3	(2,0)	787	N/A
4	(2,0)	810	N/A
5	(2,1)	844	N/A
8	(2,1)	1175	N/A
9	(2,1)	1338	1474
10	(2,1)	1388	1689
15	(3,0)	1637	1630
16	(3,0)	1645	1639
24	(3,1)	2577	2602
25	(3,1)	2606	2628
26	(4,0)	2626	2659
27	(4,0)	2635	2668

B. Experimental Validation of the Mesh-to-Mesh Projection

The methodology described in Section II is used to compute the vibration response. The mechanical FE model is illustrated in Fig. 2a: the global structure (stator + rotor + support) is considered, with spring contacts between rotor shaft and endshields, and clamped contacts between stator lamination and endshields. The natural frequencies were fitted to several

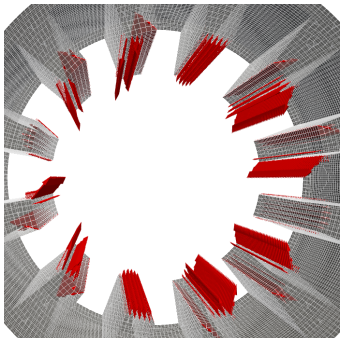

Fig. 3: Magnetic nodal forces on the mechanical mesh at $2f_s$.

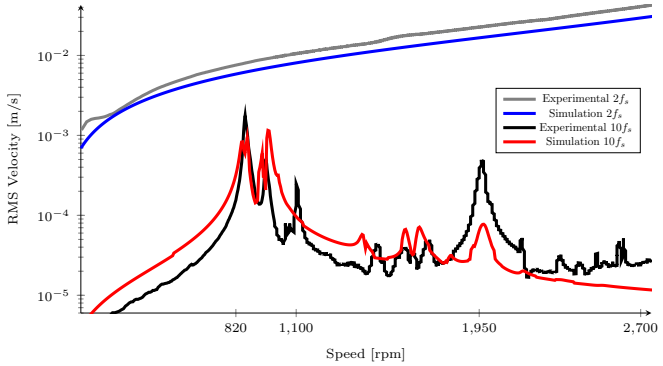

Fig. 4: Experimental run-up vibration measurements compared to simulation (load case based on mesh-to-mesh projection).

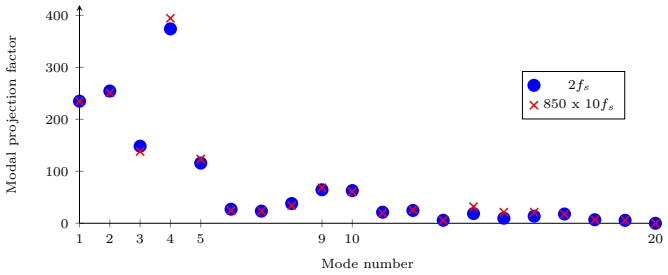

Fig. 5: Modal projection factor on each structural mode computed with numerical simulation.

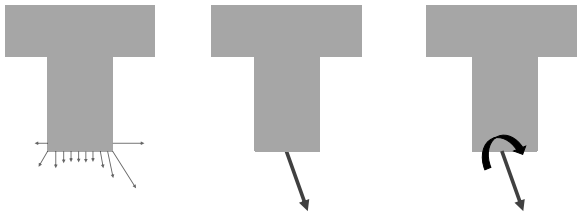

Fig. 6: Studied load cases based on VWP nodal forces: (a) distributed nodal forces (after mesh-to-mesh projection), (b) lumped force, (c) load vector (lumped force + moment).

modes obtained from the experimental modal analysis (see Table. I). An illustration of the nodal forces applied on the stator lamination at $2f_s$ is presented in Fig. 3. The outputs of interest being the order tracking vibration levels at $2f_s$ and $10f_s$ as discussed in Section III-A.

Measurements on the actual benchmark test-bed with the mounted 12s10p prototype in Fig. 2b have been performed using 5 accelerometers (1 reference and 4 measurements) randomly distributed on the outer surface of the stator lamination. The corresponding 4 closest nodes were extracted from the simulation. The comparison between numerical and experimental vibration RMS at these points are presented in Fig. 4. The comparison at $2f_s$ gives a good correlation between the simulation and the experiment with less than 1.5 dB of difference on the speed range. The comparison at $10f_s$ also gives a good correlation with fewer than 3 dB error, except at the resonance around 1950 rpm where there is an error of 8 dB. This last resonance corresponds to a mode (3,0) (see Table I). In the numerical model, the eccentricities have been neglected, explaining the differences observed with test. Indeed, magnetic forces at (10fs, $r = 2$) mainly come from a combination of the fundamental magnetic field (fs, p) and the harmonic (11fs, 11p - $4Z_s$), with $p = 5$ the pole pair number and $Z_s = 12$ the number of teeth. However, static eccentricity can generate an additional (fs, $p \pm 1$) field harmonic due to air-gap reluctance modulation. As a consequence, it can generate a wavenumber $r = 11p + (p-1) - 4Z_s = 3$, resulting in higher resonance at 1950 RPM with modes (3,0) as observed in the experimental measurements. Even without considering eccentricities, these odd modes can be excited in the simulation because of the geometrical asymmetry of the model and the numerical residuals unbalanced forces. This issue is further discussed in Section III-C. Resonance observed at 1100 RPM in the 10fs is probably due to mode (2,1) at 844 Hz which has not been fitted in the numerical model.

Further comparison can be done by computing the modal projection factor for each mode as [11]:

$$\left(\mathbf{Q}_n \cdot \hat{\mathbf{F}}\right)(\omega) = \sum_j \mathbf{Q}_n^j \hat{F}^j(\omega) \tag{16}$$

The values of modal projection factors (16) are presented in Fig. 5. In both cases, the two main excited modes are the modes n°2 and n°4 which are symmetric (2,0) ovalization modes of the yoke at natural frequencies 727 Hz and 810 Hz to be compared with the experimental natural frequencies 721 Hz and 797 Hz of the same modes. It can also be observed that the two harmonics $2f_s$ and $10f_s$ seem to have a proportional modal projection in Fig. 5: it means that despite the differences between local force distributions, the mechanical response is similar.

In the following, it is considered that the numerical model based on mesh-to-mesh projection is accurate enough to be used as a reference.

C. Lumped Tooth Force and Modulation Effect

The goal of this section is to compare the three different types of load cases illustrated in Fig. 6: the distributed nodal force in Fig. 6a corresponds to the mesh-to-mesh method presented in Section II-B, the lumped tooth force in Fig. 6b is obtained by summing up all the nodal force per tooth on the magnetic mesh, and the load vector is calculated as the lumped force and considering the resulting moment at the middle of the tooth tip. The vibration comparison is presented in Fig. 7: the lumped force load cases add 4dB at 10fs and add less than

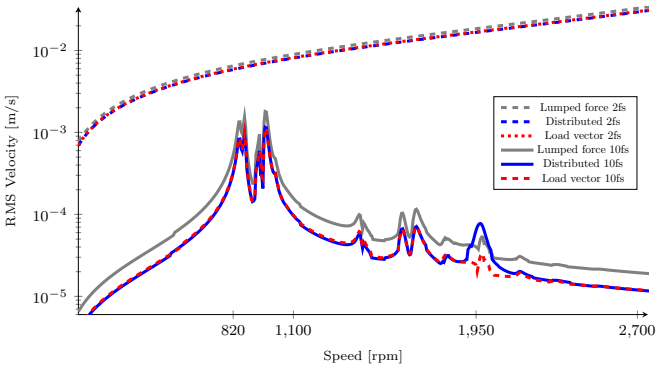

Fig. 7: Comparison of vibration amplitude depending on the type of load case.

1dB at 2fs compared to the reference distributed nodal force load case. The load vector case gives back almost the same vibration as the reference (less than 1dB difference). These results stay almost constant at every speed (or frequency).

The only significant exception appears around 1640 Hz which corresponds to the natural frequency of the modes (3,0) (see Table I). These modes are excited despite the absence of eccentricities in the model. Then, it can be assumed that this particular excitation is coming from numerical error (residual unbalanced magnetic forces). These results highlight that the mesh-to-mesh projection may amplify the unbalanced forces. This point can be verified by comparing the total force acting on the stator before and after mesh-to-mesh projection

$$F_{\text{tot}} = \sum_i F^i \; \hat{F}_{\text{tot}} = \sum_j \hat{F}^j \tag{17}$$

In this case, the total unbalanced magnetic forces amplitude at 10fs are $\|F_{\text{tot}}\| = 2e{-}5$ N and $\left\|\hat{F}_{\text{tot}}\right\| = 8e{-}2$ N. It highlights a significant risk of numerical errors with odd modes by using mesh-to-mesh projection. As a consequence, conservation of total unbalanced force should be carefully monitored when using this type of projection.

According to [4], each wavenumber can be integrated into a lumped force wave on each tooth. As a consequence, this lumped force wave might be undersampled by the number of teeth Z_s. In the studied case with $Z_s = 12$, the wavenumber $r = 10$ would be modulated into $r = -2$ as illustrated in Fig. 8. Thus, the 10fs should have a vibration response similar to the 2fs. The previous results of this study support this concept for two reasons:

- Section III-C verified the validity of the lumped tooth force load case, which is the main hypothesis of the modulation effect model,
- the 10fs has a proportional projection factor on each modes compared to the 2fs (see Fig. 5), strongly suggesting that the two different distributions of force excite the modes similarly.

Future research work should investigate the inclusion of moments in the calculations of the modulation effects.

IV. Conclusion

A complete mesh-to-mesh projection methodology has been discussed and confronted with experimental measurements on a 12s10p SPMSM electrical machine. The differences have been analyzed, and the concerns about unbalanced excitations have been raised. Then, the mesh-to-mesh projection results have been used to study the common magneto-mechanical coupling technique based on lumped tooth forces. The significant contribution of moment resultant has been highlighted in the studied case. Thus, this study suggests that the effect of small design modification on the force distribution can be accurately taken into account by using the resulting moment. Finally, all these results support the use of the modulation effect to perform e-NVH simulation. Future research work should adress the comparison with lumped force and moment calculated from the Maxwell stress tensor.

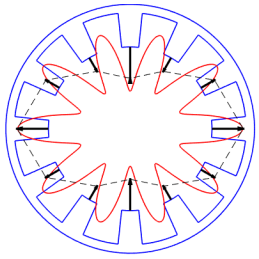

Fig. 8: Illustration of the modulation effect with an airgap wavenumber $r = 10$ modulated into a lumped force wavenumber $r = -2$.

References

[1] P. Kotter, D. Morisco, M. Boesing, O. Zirn, and K. Wegener, "Noise-vibration-harshness-modeling and analysis of a permanent-magnetic disc rotor axial-flux electric motor," *IEEE Trans. Magn.*, vol. 54, no. 3, pp. 1–4, 2018.

[2] E. Devillers, M. Hecquet, X. Cimetiere, J.-P. Lecointe, J. L. Besnerais, and T. Lubin, "Experimental benchmark for magnetic noise and vibrations analysis in electrical machines," in *Int. Conf. Elec. Mach. (ICEM)*, Alexandroupoli, Greece, Sep. 2018.

[3] A. Saito, M. Kuroishi, and H. Nakai, "Vibration Prediction Method of Electric Machines by using Experimental Transfer Function and Magnetostatic Finite Element Analysis," *J. Phys.: Conf. Series*, vol. 744, p. 012088, sep 2016.

[4] H. Fang, D. Li, R. Qu, and P. Yan, "Modulation Effect of Slotted Structure on Vibration Response in Electrical Machines," *IEEE Trans. Ind. Electron.*, vol. 66, no. 4, pp. 2998–3007, apr 2019.

[5] Z. Wang, "Contribution to finite element analysis of magneto-mechanical and magneto-thermal phenomena," Ph.D. dissertation, Université de Lille, 2013.

[6] J.-L. Coulomb and G. Meunier, "Finite element implementation of virtual work principle for magnetic or electric force and torque computation," *IEEE Trans. Magn.*, vol. 20, no. 5, pp. 1894–1896, 1984.

[7] S. Sathyan, A. Belahcen, J. Kataja, T. Vaimann, and J. Sobra, "Computation of stator vibration of an induction motor using nodal magnetic forces," in *Int. Conf. on Elec. Mach. (ICEM)*, 2016, pp. 2198–2203.

[8] R. Pile, G. Parent, Y. Le Menach, J. Le Besnerais, T. Henneron, and J.-P. Lecointe, "Effect of mesh-to-mesh projection on the magnetic tooth forces calculation in electrical machines," in *Int. Conf. on Elec. Mach. (ICEM)*, Goteborg, Sweden., Aug. 2020, pp. 2500–2506.

[9] G. Parent, P. Dular, J.-P. P. Ducreux, and F. Piriou, "Using a galerkin projection method for coupled problems," *IEEE Trans. Magn.*, vol. 44, no. 6, pp. 830–833, jun 2008.

[10] R. H. MacNeal, "A hybrid method of component mode synthesis," *Comput. & Struct.: Special Issue Struct. Dynamics*, vol. 1, no. 4, pp. 581 – 601, 1971.

[11] M. Van der Giet, *Analysis of electromagnetic acoustic noise excitations: A contribution to low-noise design and to the auralization of electrical machines*. Shaker Verlag, 2011.

[12] EOMYS ENGINEERING, "MANATEE software (v1.09.01)," 2020. [Online]. Available: https://manatee.eomys.com